POD approach for unsteady aerodynamic model updating

Fabio Vetrano, Franco Mastroddi, Roger Ohayon

POD approach for unsteady aerodynamic model updating

F. Vetrano, F. Mastroddi, R. Ohayon

Abstract A method for aerodynamic model updating is proposed in this paper. The approach is based upon a correction of the eigenvalues of the reduced-order unsteady aerodynamic matrix through an optimization with objective function defined through the difference in the generalized aerodynamic forces or on the aeroelastic poles. The high-fidelity model in reduced-order form is obtained by the proper orthogonal decomposition (POD) technique applied to the computational fluid dynamics Euler-based formulation. Many of the methods that have been developed in the past years for simpler aeroelastic models that use, for example, doublet-lattice method aerodynamics, can be adopted for this purpose as well. However, this model is not able to capture shocks and flow separation in transonic flow. The proposed approach performs the updating of the aerodynamic model by imposing the minimization of a global error between target aerodynamic performances, namely experimental performances, and an aerodynamic model in reduced-order form via POD approach. After a general presentation of the application of the POD method to the linearized Euler equations, the optimization strategy is presented. First, a simple test on a 2D wing section with theoretical biased data is performed, and then, the performances of different optimization strategies are tested on a 3D model updated by wind tunnel data.

Keywords Aeroelasticity · POD · Reduced-order model · Unsteady aerodynamic updating · WT test data

F. Vetrano (✉)
Loads and Aeroelasticity Department, Airbus,
316 Route de Bayonne, 31060 Toulouse, France
e-mail: fabio.vetrano@airbus.com

F. Mastroddi
Mechanical and Aerospace Engineering Department,
"La Sapienza" University of Rome, 18 Via Eudossiana,
00184 Rome, Italy

R. Ohayon
Structural Mechanics and Coupled System Laboratory,
Conservatoire National des Arts et Métiers, 2 Rue Conté,
75003 Paris, France

List of symbols

Ω	Computational domain volume
$\bar{W}$	Mean instantaneous field
F	Flux
N^i	Normal to the cell face
a^i	Velocity in the cell face
f, g, h	Flux component vector
ψ	Proper orthogonal mode
U	Flow field
η	Vector of the components of the disturbance field in the POD base
φ	Structural modes
d	Displacement field
q	Generalized coordinates
$\underline{f}$	Generalized aerodynamic force
$\hat{\mathrm{K}}$	Stiffness matrix
$\hat{\mathrm{M}}$	Mass matrix
$\hat{\mathrm{C}}$	Damping matrix
M	The instantaneous position of the grid nodes
a_0, a_1	Fluid system matrix
b_0, b_1	Coupling vector
a	Reduced-order aerodynamic matrix
V	Right eigenvector
λ	Aeroelastic poles
μ	Complex aerodynamic poles
r	Design variable for real part
s	Design variable for complex part

1 Introduction

During the last two decades, the evolution of computing capabilities has made possible the use of computational fluid dynamics for industrial processes. An accurate model is essential to study and develop new civil transportation aircraft. To build a high-fidelity aeroelastic model in the transonic regime for load calculations and aeroelastic application (flutter, gust response, etc.), the use of the CFD has become a superior choice over the DLM or methods derived from piston theory. However, many engineering and industrial problems solved by the CFD involved fluid–structure interaction and required a very large number of degrees of freedom—typically in terms of millions—and also a large number of simulation parameters are involved in the computing process. Thus, due to the computational cost, the potential of the CFD code is currently limited to the analysis of a few configurations. For this reason, the DLM approach and related correction techniques are today widely used in industrial processes. Although the computational cost of this approach is minimal and its robustness has been proved over the past years, the DLM method cannot cover every physical phenomenon which can instead be evaluated by a CFD calculation. For this purpose, several reduced-order modelling techniques have been developed in this domain. The objective of these techniques is to build a simple fluid dynamics model with a significant reduction of the degrees of freedom representative of the high-fidelity model. The Karhunen–Loève decomposition, also known as proper orthogonal decomposition, is a powerful method for determining an optimal reduced-order aerodynamic model in terms of energy to represent a sample set of data and build a reduced-order model [10, 11, 15–17, 21, 22].

Since the first use of the DLM approach, many efforts have been made to widen the applicability scope of the theory and several extensions of the standard calculation methods are proposed [12–14]. It was finally accepted in aerospace industries that the only way to go beyond these limits (transonic regime, prediction of aerodynamic forces on control surfaces, effects of thickness and viscosity) was the introduction of a posteriori corrections on results. Corrections of linear results are typically performed by means of pre-multiplying diagonal-correction matrices applied either to the pressure vector at the DLM boxes or to the downwash vector. Those corrections are carried out by means of data obtained with more accurate methods. Several correcting methods can be found in the literature. The first correction technique was proposed by Yates and Bergh [4] and after by Rodden and Giesing [3], Goodman [5], Garner Luber and Schmid [2]. All these methods use experimental data to correct the linear theory. Indeed, the evolution of computing capabilities has made possible the use of unsteady CFD results and several correcting methods have been developed to improve linear results using these data [6, 7]. Recently, a direct correction of aerodynamic influent coefficient matrix, obtained by DLM approach, by scaling factor for precise flutter prediction has been also proposed in [8]. Similar corrections, in the neighbourhood of transonic regime, have also been provided by ZTRAN tool included in ZONA code [19]. Some other different ways of improving the accuracy of the aeroelastic model have been proposed recently, coupling the advantages of the reduced-order model with the correction techniques: Hu et al. [9] proposed an aeroelastic model updating based on Kriging multi-fidelity modelling and physics-based modified computational model coupled with a POD approach combined with an harmonic-balance method, by incorporating wind tunnel and flight test data at the same time. In the present paper, the parameters of the eigenproblem associated with the POD approach has been used as design variables to optimize the updating problem of the ROM model with respect to the experimental test or reference high-fidelity CFD models so assuring a good capability in the updating process itself. More specifically, a new alternative strategy to incorporate information coming from experimental test or CFD calculations to improve the aeroelastic POD/ROM model is demonstrated. The block diagram of the proposed updating process is presented in Fig. 1. Specifically, the present research is within the framework of the AMMAT project (aeroelastic model matching and test), which is an Airbus research programme. The first aim of AMMAT is to improve the aeroelastic model quality for a fine flight control system

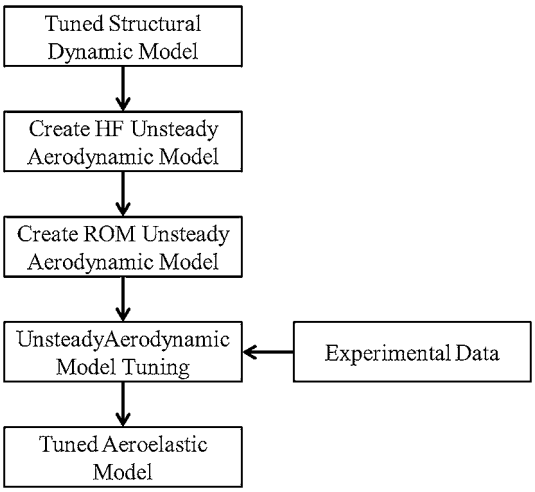

Fig. 1 Block diagram for unsteady aerodynamic tuning

design and, consequently, for loads and aeroelastic purposes involving structural dynamics. We deal with structural dynamics model in-flight, and our first purpose is to get a high quality transfer function between control surface and control laws sensors, and this is compulsory for flight control system (FCS) development and certification. The correlation between experimental data and theoretical data is of premium importance in aircraft development. It allows us to check whether the theoretical model is close to reality. The theoretical model is used to tune FCS, to perform aircraft certification in the loads and aeroelasticity domain. Many loads cases, like continuous turbulence, cannot be easily tested in flight, and we rely on the theoretical model to evaluate them. The tuning process gives information on errors present in the model, validates the modelling used in the model and can give uncertainties values to be used for future aircraft development.

Some improvements in the structural dynamics test process may be the outcome of the AMMAT research. In particular, a methodology based on flight test data to tune the aeroelastic model in-flight has been proposed within the project, and if successful, this could lead to a reduction or elimination of the GVT test, while increasing model quality.

In the present paper, the theoretical basis for building an aeroelastic POD Galerkin ROM from linearized Euler equation is presented in Sect. 2. In Sect. 3, some remarks on the proposed unsteady aerodynamic updating strategies are shown. In Sect. 4, the numerical results on NACA wing section and on wind tunnel model are presented, and finally, in Sect. 5, some conclusions are given.

2 Theoretical background

In this section, the physical model used, together with its suitable reduction, has been shown. Specifically, in Sect. 2.1, the Euler model is presented. In Sect. 2.2, the ROM approach on the aerodynamics based on POD analysis is carried out. Finally, the overall reduced aeroelastic model is presented in Sect. 2.3.

2.1 Linearized Euler CFD model

A viscous and heat-conducting flow is most accurately modelled by the Navier–Stokes equations. However, if the Reynolds number is sufficiently high, the Prandtl number is of order unity, and separation does not occur. Thus, the viscous and heat transfer effects are confined to narrow regions near the airfoil surfaces and the wakes. Under these circumstances, the Euler equations are a good approximation for modelling the behaviour of the flow. The unsteady Euler equations are the starting point of the linearized Euler analysis.

In this paper, the flow is assumed to be governed by the linearized Euler equations (LEE) in a moving mesh grid (arbitrary Lagrangian–Eulerian formulation) for steady and unsteady small-disturbance inviscid flows. For the sake of brevity, we will only report the principal step of the Euler equation linearization process. For more details, see [18].

Let $\mathrm{C}(t)$ be an elementary hexahedral cell of the computation domain with volume $\Omega(t)$. The faces of the cell are noted $\Gamma_i(t)$ (with $i = 1, 6$). The mean instantaneous field in the cell is defined by:

$$\bar{W} = \frac{\int_{C(t)} W \, \mathrm{d}\omega}{\Omega(t)}.$$

The discretized formulation of the Euler equations is given by:

$$\frac{\mathrm{d}}{\mathrm{d}t}(\Omega(t)\bar{W}) + \sum\nolimits_i F_i(\bar{W}) = 0. \tag{1}$$

The geometric conservation law is written:

$$\frac{\mathrm{d}}{\mathrm{d}t}(\Omega(t)) + \sum\nolimits_i \left(a^i(t) \cdot N^i(t)\right) = 0 \tag{2}$$

To linearize Eqs. 1 and 2, the mean instantaneous field $\bar{W}$ is divided into a steady mean field $\bar{W}_s$ and a fluctuation $\delta\bar{W}$:

$$\bar{W} = \bar{W}_s + \delta\bar{W}. \tag{3}$$

Similarly, the instantaneous position of the grid nodes is divided into a steady part and a fluctuation around a steady state:

$$M(i) = M_s + \delta M(t). \tag{4}$$

If a periodic solution with period T is sought, fluctuation $\delta M(t)$ around steady state M_s is periodic and centred which means $\delta M(t+T) = \delta M(t)$. The assumption made is that low amplitude fluctuations $\delta M(t)$ (first order) of the grid create fluctuations δW of the field which are of the same order of magnitude.

A Taylor series expansion around the steady solution is performed on Eq. 1, on the geometric terms (volume, normal) and on the flow terms. Only the fist-order terms are used to obtain the discretized formulation of the linearized Euler equation on moving grid:

$$\frac{d}{dt}(\Omega_s\delta\bar{W}+\delta\Omega(t)W_s)+\sum_i\left(\frac{1}{2}(f(\bar{W})+f(\bar{W}_{si}))N_x^i(t)+(g(\bar{W})+g(\bar{W}_{si}))N_y^i(t)+(h(\bar{W})+h(\bar{W}_{si}))N_z^i(t)\right.$$
$$+\frac{1}{2}([A](W_s)\delta W+[A](W_{si})\delta W_i)N_{sx}^i+\frac{1}{2}([B](W_s)\delta W+[B](W_{si})\delta W_i)N_{sy}^i \quad (5)$$
$$\left.+\frac{1}{2}([C](W_s)\delta W+[C](W_{si})\delta W_i)N_{sz}^i a^i(t)\cdot N_s^i(t)\frac{1}{2}(\bar{W}+\bar{W}_i)\right)=0$$

where the sub-index s indicates the reference steady values. The above equations system can be written as:

$$[A_0(W_s)]\delta W+[A_1(W_s)]\frac{\partial\delta W}{\partial t}=B_0(M_s)+B_1\left(\frac{\partial\delta M}{\partial t}\right) \quad (6)$$

where $[A_0(W_s)]$, $[A_1(W_s)]$ are real matrices and $B_0(M_s)$, $B_1\left(\frac{\partial\delta M}{\partial t}\right)$ are real vectors.

Euler equations are solved on a multi-block structured mesh using the Jameson-Lerat scheme introduced in the computer code REELC developed at ONERA [20].

2.2 POD Galerkin reduced-order model

Reduced-order modelling with POD is essentially based on a spectral method. By using spectral methods, field variables are approximated using expansions involving chosen sets of basis functions. The resulting Galerkin-type equations obtained by projecting Eq. 6 on such basis functions are manipulated to obtain sets of equations for the coefficients of the expansions that can be solved to predict the behaviour of field variables in space and time. The POD basis is derived from a set of system observations. In short, samples, or snapshots, of system behaviour are used in a computation of appropriate sets of basis functions to represent system variables. The POD is remarkable in that the selection of basis functions is not just appropriate, but optimal, in a sense to be described further. The need to obtain samples of system behaviour to construct the POD-based ROM is both a strength and a weakness of the method. One strength is that models can be efficiently tuned to capture physics in a high-fidelity model. Two noteworthy weaknesses are the need to compute samples with a high-order, high-fidelity method, and the possible lack of model robustness to changes in parameters that govern system behaviour. Generally, the pay-off in applying POD is quite high when, following an initial computational investment, a compact ROM can be constructed that can be used many times in a multidisciplinary environment and which is valid over a useful range of system states [23]. In the following, we will show the different steps for building an aeroelastic POD-based reduced-order model.

After having computed the POD basis (some details on POD basis evaluation have been reported in "Appendix"), the next step consists of projecting the governing fluid equation onto the reduced base. If we consider a disturbance field such as:

$$U=[\psi]\eta \quad (7)$$

η represents the vector of the components of the disturbance field in the POD base. Thus, the reduced system is obtained by projecting the linearized Euler equation into the POD basis:

$$[\psi]^H\left([A_0]U+[A_1]\frac{\partial U}{\partial t}\right)=[\psi]^H\left(B_0(d)+B_1\left(\frac{\partial d}{\partial t}\right)\right) \quad (8)$$

where H is the Hermitian operator.

The reduced-order model obtained is:

$$[a_0]\eta+[a_1]\frac{\partial\eta}{\partial t}=b_0(d)+b_1\left(\frac{\partial d}{\partial t}\right) \quad (9)$$

with $[a_0]=[\psi]^H[A_0][\psi]$, $[a_1]=[\psi]^H[A_1][\psi]$, $b_0=[\psi]^H[B_0][\psi]$ and $b_1=[\psi]^H[B_1][\psi]$. It has to be noticed that the fluid system matrix $[a_0],[a_1]$ and the coupling vector b_0,b_1 can be significantly smaller than their full-order counterparts. For more theoretical details on the Galerkin projection presented, see [1, 24].

Once the fluid ROM has been calculated, the corresponding aerodynamic forces may be determined. The displacement field d is linked to the structural modes $[\varphi]$ using the structural modal expansion

$$d=[\varphi]q \quad (10)$$

where q represents the generalized coordinates. For each structural mode φ_m, vectors $b_0(\varphi_m)$ and $b_1(\varphi_m)$ can be calculated. These vectors are stored in columns in matrix $[b_0]$ and $[b_1]$. The reduced-order model is:

$$[a_0]\eta+[a_1]\frac{\partial\eta}{\partial t}=[b_0]q+[b_1]\frac{\partial q}{\partial t} \quad (11)$$

where all the matrices are now constant with respect to the displacement. The variation of the pressure field caused by a mode of the POD basis is independent of the boundary conditions applied to the structure. This means that we can

generate a vector of generalized aerodynamic forces (GAFs) projecting the vector field generated by the motion of any POD mode on any structural mode. These vectors are collected by columns in a matrix $[F]$. Thus, the generalized aerodynamic forces are then related to the vector η by:

$$\underline{f} = [F]\eta. \tag{12}$$

2.3 Coupled fluid/structural aeroelastic model

In summary, the POD method outlined above leads to a reduced-order basis that can be used for building an aerodynamic ROM for a given free stream Mach number and angle of attack. The corresponding aeroelastic system is obtained by coupling the Eqs. 11 and 12 with the equation for a coupled fluid–structure aeroelastic system. The motion of an elastic body with respect to an equilibrium un-deformed reference position, in time domain, is described by the Lagrange equation

$$\sum_m^M \hat{M}_{\mathrm{nm}}\ddot{q}_m + \sum_m^M \hat{C}_{\mathrm{nm}}\dot{q}_m + \sum_m^M \hat{K}_{\mathrm{nm}}q_m + \frac{1}{2}\rho_\infty V_\infty^2 \underline{f} = 0 \tag{13}$$

with $\hat{C}_{\mathrm{nm}} := 2\zeta_m\sqrt{\hat{K}_{\mathrm{nm}}\hat{M}_{\mathrm{nm}}}\delta_{\mathrm{nm}}$ and where δ_{nm} is the Kroneker symbol, q are the generalized modal coordinates, $\hat{K}_{nm}$ is the stiffness matrix, $\hat{M}_{\mathrm{nm}}$ is the mass matrix associated with the chosen Lagrangian model variable, $\hat{C}_{\mathrm{nm}}$ is the damping matrix, and $\underline{f}$ is the generalized aerodynamic force vector. If we put the aeroelastic equation and the POD equation in the same equation system, we obtain the following linear system, thus any stability study is reduced to solve a standard eigenproblem for λ and u for the generalized linear system.

$$\begin{pmatrix} 0 & [I_d] & 0 \\ [-k] & [-c] & \frac{1}{2}\rho_\infty V_\infty^2[F] \\ [-b_0] & 0 & [-a_0] \end{pmatrix} u = \lambda \left(\begin{bmatrix} [I_d] & 0 & 0 \\ 0 & [m] & 0 \\ [-b_1] & 0 & [a_1] \end{bmatrix} \right) u \tag{14}$$

Note that the GAF matrix defined as the matrix relating in the frequency domain the modal co-ordinates q's with the GAF force vector $\underline{f}$ is given by

$$\mathrm{GAF}^{\mathrm{POD}} = [F]([a_0] + j\omega[a_1])^{-1}([b_0] + j\omega[b_1]). \tag{15}$$

3 Unsteady aerodynamic updating strategies

Two techniques have been proposed and developed to update unsteady aerodynamic models. The first one is based on updating the GAF matrix obtained by POD approach (see Eq. 15) with the generalized aerodynamic force obtained by the high-fidelity model. The second one is based on matching the measured and numerical frequencies and damping for each aeroelastic mode of an aircraft for different total pressure conditions. On defining the optimization problems, the parameters of a suitable eigenproblem associated with the unsteady aerodynamic ROM model are considered as design parameters of the updating process. Indeed, design variables in this reduced-order unsteady aerodynamic model tuning are scaling factors for all complex eigenvalues of the reduced-order aerodynamic matrices. The reduced-order aerodynamic matrix at a given frequency ω can be written as:

$$a(\omega) = [a_0] + j\omega[a_1]. \tag{16}$$

The eigenvalues and eigenvectors associated with $a(\omega)$ are obtained by:

$$a(\omega)V = V\mu \tag{17}$$

where several eigenproblems can be associated for any frequency ω_i. μ are the complex eigenvalue diagonal matrix and V are the complex right eigenvector matrix. The eigenvalue matrix can be written as:

$$\mu = \begin{bmatrix} \mu_{R_{11}} & \cdots & 0 \\ \vdots & \ddots & \vdots \\ 0 & \cdots & \mu_{R_{nn}} \end{bmatrix} + j \begin{bmatrix} \mu_{I_{11}} & \cdots & 0 \\ \vdots & \ddots & \vdots \\ 0 & \cdots & \mu_{I_{1n}} \end{bmatrix} \tag{18}$$

where n is the number of POMs chosen to build the reduced-order model, and $\mu_{R_{ij}}$ and $\mu_{I_{ij}}$ are, respectively, the real part and imaginary part of the eigenvalues. Design variables are defined as multipliers of the eigenvalues such that the optimized new eigenvalues matrix $\tilde{\mu}$ is given by

$$\tilde{\mu} = \begin{bmatrix} r_{11}\mu_{R_{11}} & \cdots & 0 \\ \vdots & \ddots & \vdots \\ 0 & \cdots & r_{nn}\mu_{R_{nn}} \end{bmatrix} + j \begin{bmatrix} s_{11}\mu_{I_{11}} & \cdots & 0 \\ \vdots & \ddots & \vdots \\ 0 & \cdots & s_{nn}\mu_{I_{nn}} \end{bmatrix} \tag{19}$$

where r is the design variable for the real part of the eigenvalues and s is the design variable for the imaginary part of the eigenvalues. Update eigenvalues can be written as:

$$\tilde{\mu} = \mu + \delta\mu \tag{20}$$

Thus, it is now possible to reconstruct the updated aerodynamic matrix $\tilde{a}$ for any frequency ω as shown:

$$\tilde{a} = V\tilde{\mu}V^{-1}. \tag{21}$$

It is now possible to solve the linear system and calculate the new generalized aerodynamic force.

3.1 generalized aerodynamic force tuning

Strategy 1: Try to find the solution, in the objective space, that minimizes the distance between the GAF matrix as

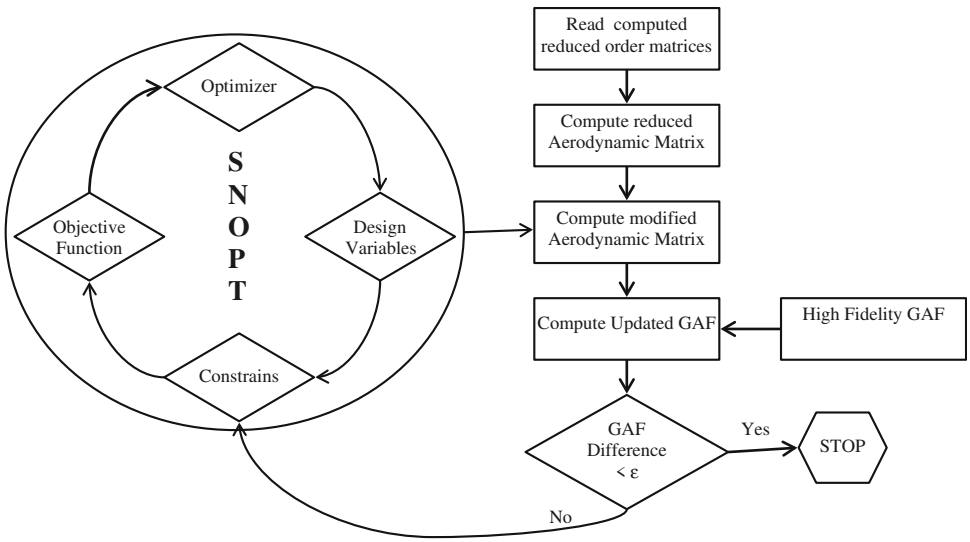

Fig. 2 Block diagram for generalized aerodynamic force tuning

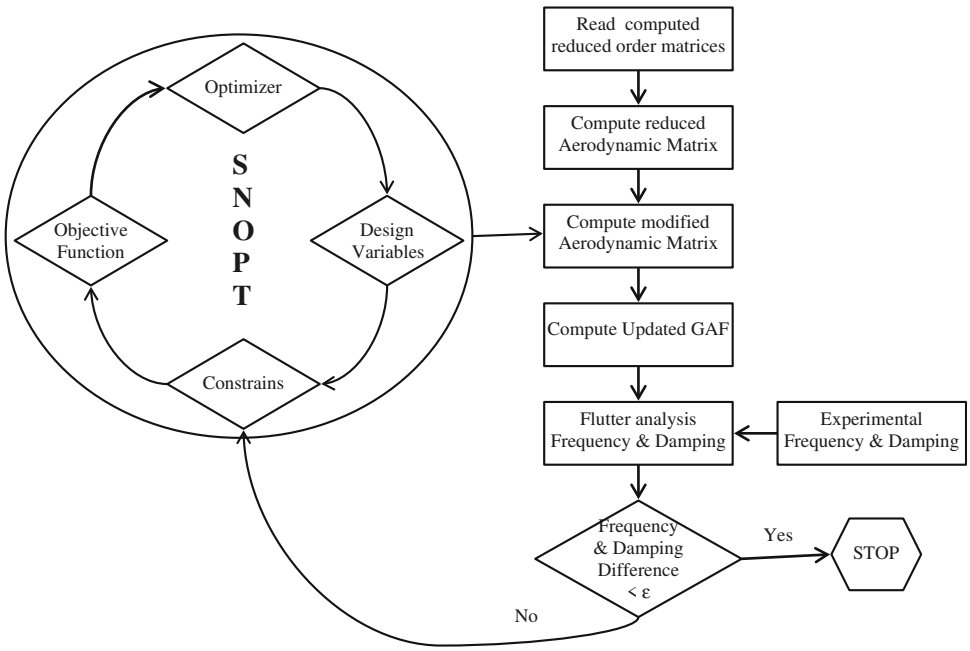

Fig. 3 Block diagram for frequencies and damping tuning

obtained by direct CFD analysis ($\mathrm{GAF}^{\mathrm{CFD}}$) and by POD modelling ($\mathrm{GAF}^{\mathrm{POD}}$, Eq. 15) with updating strategies. For example, it is possible to solve the problem:

$$\min d(x) = \left\| \mathrm{GAF}^{\mathrm{POD}} - \mathrm{GAF}^{\mathrm{CFD}} \right\|_p \tag{22}$$

where p indicates the norm type of a vector to be minimized varying the design vector x composed by r and s multiplying coefficient defined in Sect. 2.1 standard optimizer toolbox has been used [25]. Figure 2 shows some descriptive details of the optimization algorithm.

3.2 Frequencies and damping tuning

Strategy 2: Try to find the solution, in the objective space, that minimizes the distance between the poles of the aeroelastic system as obtained, for example, by experimental data (wind tunnel or flight test data) and by ROM–POD modelling with updating strategies based on Eqs. 12, 13 and 14. A norm vector for the aeroelastic pole differences will be minimized (see later) varying the design vector x composed by r and s multiplying coefficients defined in Sect. 2 (Fig. 3).

All the solution methods proposed are based on the idea of transforming the original multi-objective problem into a single objective problem (transform the vector problem of minimizing the distance between each aeroelastic pole into a scalar problem). The methods are classified into three categories: method without preference, a posteriori method and a priori method, as in the following.

Approach 1: distance method or goal method (without preference): Try to find the solution, in the objective space, that minimizes the distance between the admissible region (Z) and any reference point $z^{\text{ref}} \notin Z = f(\mathcal{F})$. For example, if $z^{\text{ref}} = z^{\text{id}}$, it is possible to solve the problem:

$$\min d(x) = \left\| f(x) - z^{id} \right\|_p \quad \mathcal{F} = \{x \in R^n; g(x) \leq 0\} \tag{23}$$

where

$$\|x\|_p = \left(\sum_{i=1}^{k} |x_i|^p \right)^{1/p} \tag{24}$$

where p is the standard norm of a vector.

Approach 2, ε constraints method or trade-off method (a posteiori): Choose an objective function $f_l(x)$ and transform the other objective functions $f_i(x)$ with $(i = 1, 2, \ldots, k, i \neq l)$ to constraints and impose the upper bound ε_i. Thus, the scalar problem to solve is:

$$\begin{aligned} &\min f_l(x) && l \in \{1, 2, \ldots, k\} \\ &f_i(x) \leq \varepsilon_i && \forall i = 1, 2, \ldots, k, i \neq l \\ &g(x) \leq 0. \end{aligned} \tag{25}$$

*Approach 3, hierarchical method (*a priori*):* Order the objective functions on the strength of relevance (for instance, in the present case, the description of a specific aeroelastic pole-mode could be more relevant with respect to the others). After classifying the objective functions, the solution process starts with the minimization of the first (more relevant) objective function $f_1(x)$ in the original admissible region $\boldsymbol{F}$. Thus, the scalar problem to solve is:

$$\begin{aligned} &\min f_1(x) \\ &g(x) \leq 0. \end{aligned} \tag{26}$$

If the problem above has a unique solution, this is also the solution of the optimization problem and the algorithm stops. Otherwise, we try to minimize the second objective function $f_2(x)$ following the order choice during the classification but adding to the original constraints other constraints that assure that the new solution does not worsened the value of the first objective function. Thus, the scalar problem to solve is:

$$\begin{aligned} &\min f_2(x) \\ &f_1(x) \leq f_1\left(x_1^*\right) \\ &g(x) \leq 0 \end{aligned} \tag{27}$$

where x_1^* is the solution of the first problem. If the problem above has a unique solution, the algorithm stops. Otherwise, we can restart the procedure by selecting the next objective function in the ranking. At the generic step $h \leq k$, we can write:

$$\begin{aligned} &\min f_h(x) \\ &f_i(x) \leq f_i\left(x_i^*\right) \qquad i = 1, 2, \ldots, h-1 \\ &g(x) \leq 0 \end{aligned} \tag{28}$$

where x_i^* is the solution of the *i th* problem. The added upper bound can be a fraction of the optimal solution $f_i\left(x_i^*\right)$ found during the optimization process:

$$f_i(x) \leq \left(1 - \frac{\varepsilon_i}{100}\right) f_i\left(x_i^*\right) 0 \leq \varepsilon_i \leq 100. \tag{29}$$

4 Numerical results and discussion

A critical review of the optimization strategy is now applied to two different aeroelastic systems, a NACA 64A010 wing section and a transonic wind tunnel model representative of an Airbus commercial aircraft.

4.1 NACA 64A010 wing section

The aeroelastic full-order computational model consists of a CFD structured Euler C-mesh with 6,888 cells, which corresponds to 27,552 flow perturbation unknowns (see Fig. 1a), and two structural modes, obtained by a vertical rigid translation (Fig. 1b) and a pitch rotation around the quarter chord (Fig. 1c) of the aerodynamic mesh. For all simulations, total pressure and total temperature are fixed, respectively, at 203,321 Pa and 310 Kelvin degrees, the Mach number is fixed at 0.7. POD basis vectors were calculated using a frequency domain method of the snapshot approach. The reduced frequency k is defined as:

$$\mathrm{k} = \omega c / U \tag{30}$$

where ω is the frequency of the airfoil motion, c is the wing section chord and U is the freestream velocity. In order to compute the POD basis vectors, flow snapshots are evaluated at 11 evenly spaced reduced frequency between 0 and 0.3 for each structural mode for a total of 44 real POD vectors (2 modes × 11 frequencies × real and imaginary part of the snapshots) (Fig. 4).

Since the snapshots are computed, we then use the technique described in Sect. 2.2 to find the POD vectors. Figure 5 shows the proper orthogonal values (POV) distribution or σ eigenvalues of the correlation matrix. One sees that the vast majority of the energy (99 %) is contained in the first 10 POD vectors.

Once the POD basis has been built, the method shown in Sect. 2.2, to calculate the generalized aerodynamic forces is applied.

The first model updating is performed using the first strategy proposed for matching of the generalized

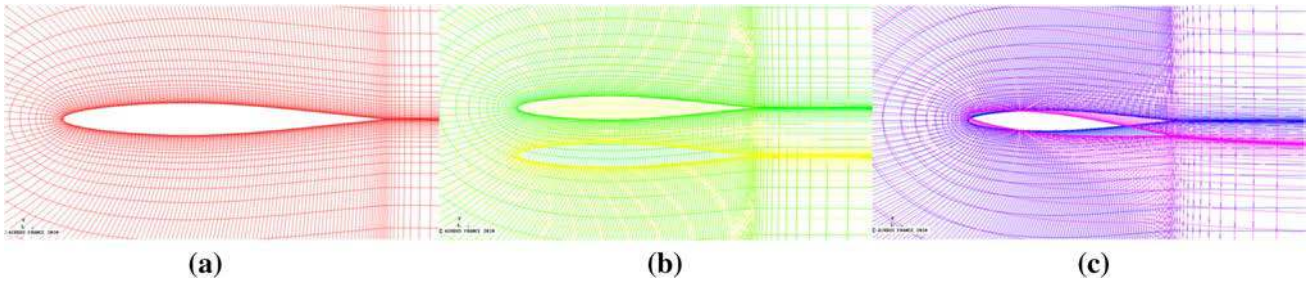

Fig. 4 Computational grid for NACA 64A010 airfoil. **a** Mesh near the airfoil, **b** vertical rigid translation, **c** 1/4 chord pitch rotation

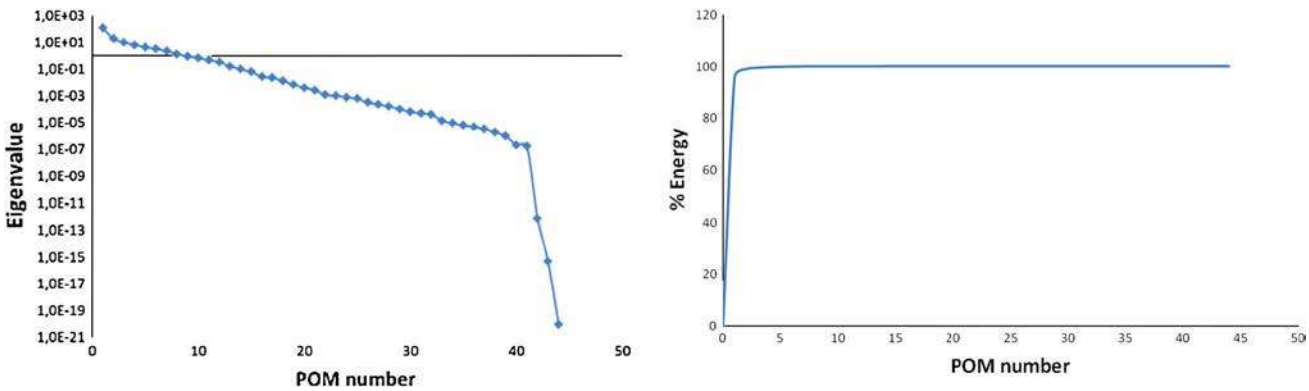

Fig. 5 Eigenvalues λ/% energy distribution of the POM vectors computed for the NACA 64A010

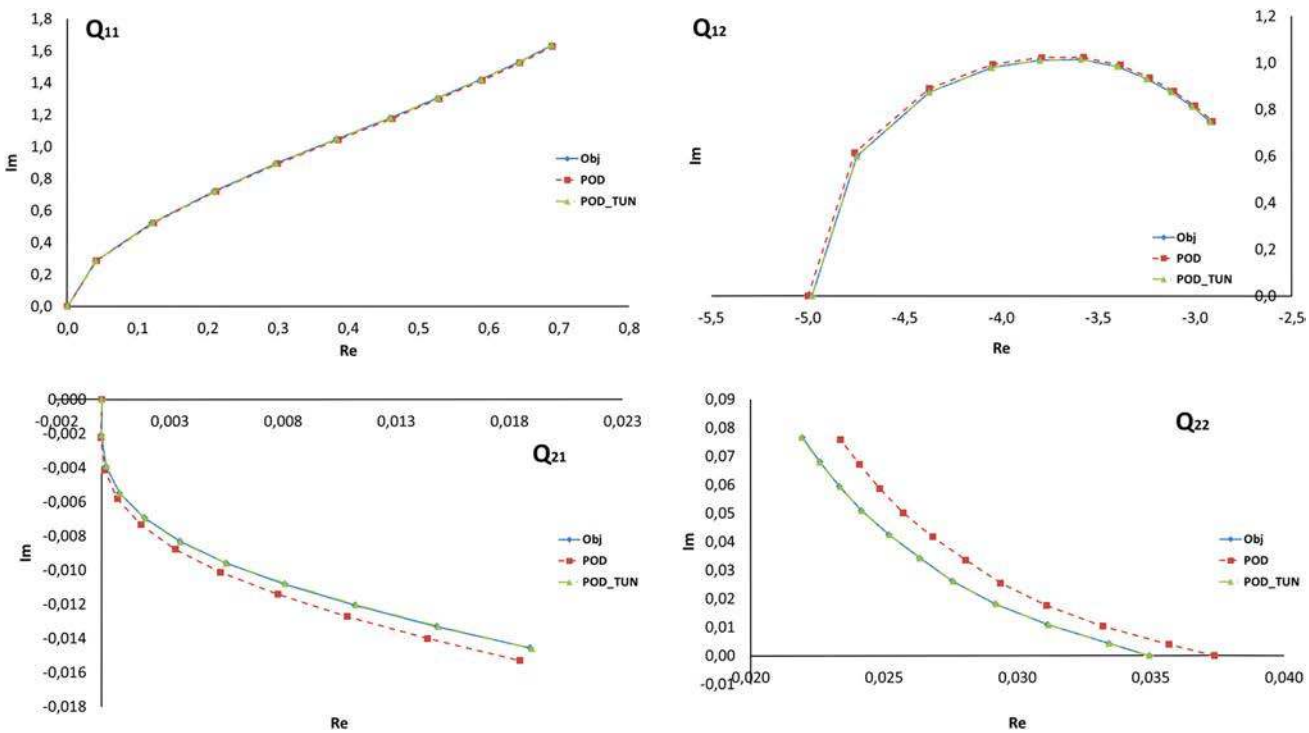

Fig. 6 GAF NACA64A010 comparison using Strategy 1 updating approach

Table 1 Error for poles using Strategy 2

Pressure	Error before (%)		Error approach 1 (%)		Error approach 2 (%)		Error approach 3 (%)	
	Frequency	Damping	Frequency	Damping	Frequency	Damping	Frequency	Damping
10,000	0.43	0.41	0.09	0.45	0.01	0.01	0.01	0.01
15,000	0.49	0.41	0.05	0.49	0.02	0.00	0.04	0.02
10,000	0.03	0.64	0.01	0.69	0.01	0.36	0.01	0.55
15,000	0.03	1.17	0.01	1.10	0.00	0.20	0.00	0.24

aerodynamic force obtained by POD approach and the generalized aerodynamic force obtained by the high-fidelity model via a direct CFD simulation. The reduced aerodynamic matrix is parameterized, as shown in Sect. 3, using 84 design variables for each reduced frequency. The variation of the design variables (r and s coefficient vectors in Eq. 19) is limited to 10 %, and the variation of the modified GAF is limited to 10 %. After the updating process, a check of the new unsteady pressure distribution computed is carried out to verify the correct reconstruction of the unsteady pressure field. In Fig. 6, the evaluated GAFs are compared with the reference solution: the figure shows a difference between the GAF obtained by the POD method and the GAF obtained by the high-fidelity model. After the updating process, the updated GAF is superimposed to the high-fidelity GAF. To obtain the convergence of the objective function, we need 2100 iteration for a computational cost of about 5 min in a conventional desktop computer. The maximal variation of the design variable is of $+1.84$ % with respect to the original value and the minimal variation of the design variable is -1.75 % with respect to the original value.

In the second model, updating is performed using the second strategy proposed for matching of the frequencies and damping of the aeroelastic system obtained by POD approach with the frequencies and damping obtained by the high-fidelity model. No experimental data on frequency and damping was available for NACA64A010 test case, and thus, to obtain a dummy frequency and damping for the updating process, the original generalized aerodynamic force was ad hoc modified. In particular, four terms of the high-fidelity GAF matrix are randomly altered by multiplying the original terms for a correction coefficient of $+15$ or -15 %. After having calculated the objective values for the optimization, the three strategies proposed in Sect. 3.2 are applied and critically evaluated.

In Table 1, we can see the comparison between the results obtained after the updating process using the three strategies proposed, before the updating process and the reference, in terms of the percentage error frequency and damping, with respect to the reference values, for two different total pressure conditions. From the analysis of the results, it is possible to see that even before updating the POD model gives very good results in terms of frequency and damping. To obtain the right convergence level of the updating process ($\varepsilon < 1.E\text{-}04$ see Fig. 3), we need between 4,000 and 4,500 iterations, for the three strategies, for a computational cost of about 3/4 min in a standard computer desktop. The maximal variation of the design variable found during the updating process, for the three strategies, is of $+2.15$ % with respect to the original value and the minimal variation of the design variable is -2.25 % with respect to the original value.

Regarding the error before updating, we can see a 0.4 % error for frequency and damping for the first structural mode, a 0.02 % error for the frequency of the plunging mode, an error of 0.64 % for the damping at the first total pressure condition and an error of 1.17 % for the damping at the second total pressure condition. After the updating process for the approach 1, we can see a general improvement of the accuracy in terms of frequency, faced with a slight deterioration in terms of damping. At this time, it is pertinent to point out that only the frequencies are included in the cost function to be optimized. Regarding the approach 2, after the updating process, we can see a general improvement of the accuracy of the results. In particular, a very strong improvement in terms of frequency is obtained, the percentage error is reduced to 0.01–0.02 % for all pressure conditions and also a significant reduction of the error for damping is obtained. The percentage error for the first mode is reduced to 0.01 %, and for the second mode, it is reduced to 0.36 % for the first pressure condition and 0.2 % for the second pressure condition. After the updating process for approach 3, we can see a very strong improvement in terms of frequency is obtained. The percentage error is reduced to 0.01–0.04 % for all pressure conditions and also a significant reduction of the error for damping is obtained, and the percentage error for the first mode is reduced to 0.01 % and for the second mode is reduced to 0.55 % for the first pressure condition and 0.24 % for the second pressure condition.

In Fig. 7, a comparison between the generalized aerodynamic force obtained after the updating process by the three approaches (see legend for details) and the

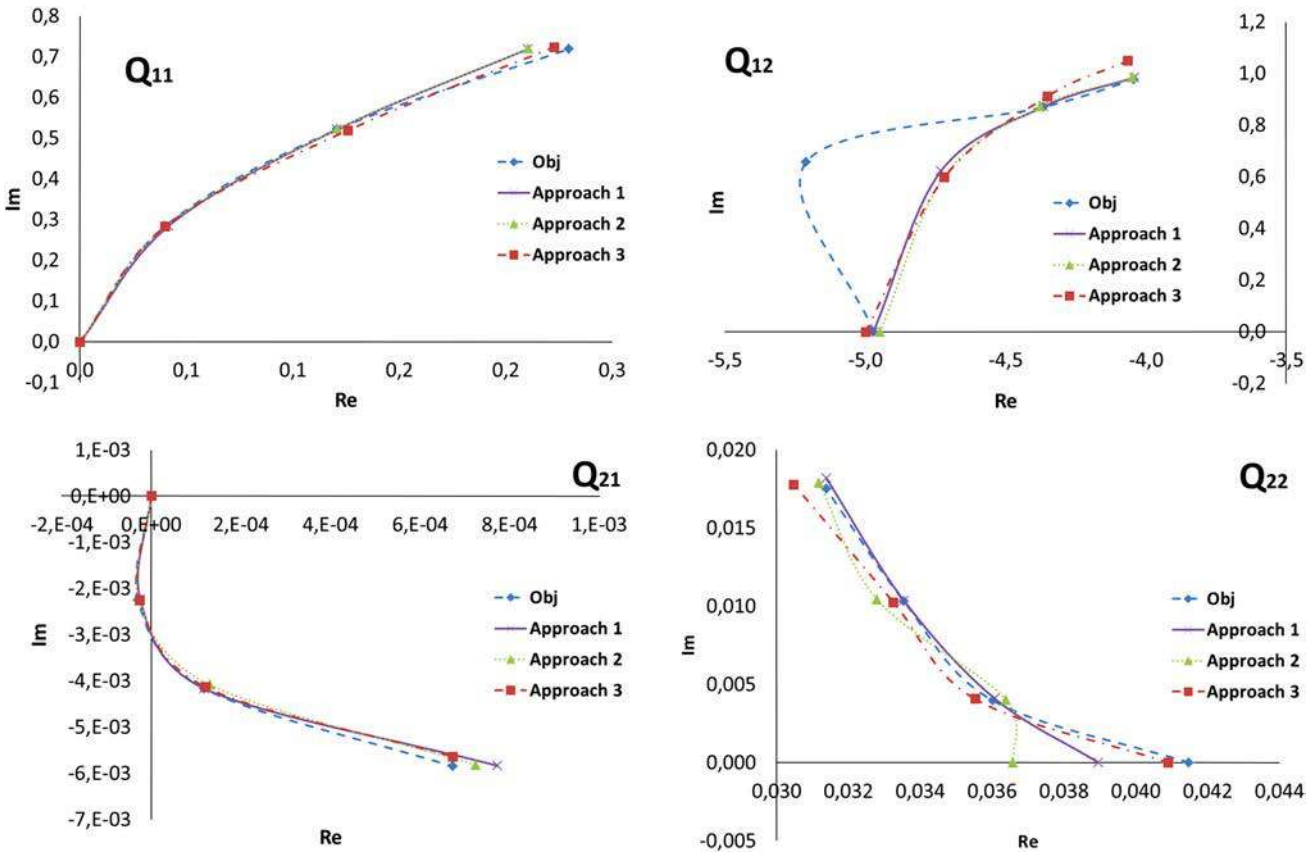

Fig. 7 GAF results comparison using Strategy 2

generalized aerodynamic force of reference is proposed. We can see a very good tracking for the GAF 1:1 (upper left curves) and 2:1 (lower left curves) obtained by the updated model and not very good accuracy for the second frequency of the GAF 1:2 (upper right curves) and for the first frequency of the GAF 2:2 (lower right curves), only the approach 3 seems to give a good tracking, with a little left shift of the GAF 2:2.

As concluding remarks for this Section, it can be pointed out that the first strategy is able to globally give a very good accuracy for fitting the target results (GAF matrix) employing a slight computational cost. Regarding the second strategy proposed, we can say that the approach 1 is the less efficient, due to the fact that in the objective function, only the frequencies are take into account, and the approaches 2 and 3 are able to globally give the same accuracy for fitting the target results (aerodynamic poles), employing essentially the same computational efforts.

4.2 AMP model

The next example refers to a representative Airbus commercial model that was tested in a transonic wind tunnel. It is also known as AMP model [26] (see Fig. 8a). The AMP wing-fuselage configuration has been used to validate the updating approach. The AMP wing test programme was worked out in 1990, jointly by AIRBUS, DASA, DLR and ONERA. The objective of this programme was to study the flutter behaviour of a model aircraft in the transonic domain. Two models (half wing-fuselage configuration), with identical geometric shapes, were tested in the S2 wind tunnel of Modane. The first model, also known as pressure model, was used to study the steady and unsteady pressure fields and the static and dynamic wing deformations. The second model, also known as flutter model, was employed for flutter investigation. The wing is equipped with 288 Kulite pressure sensors, distributed on the upper and lower surfaces in 10 sections. Ten optical fibres, located along the leading edge and trailing edge of the wing, are used for measurement of the static deformations. Extensive aerodynamic and structural experimental data are available for this wing for a wide range of test conditions, ranging from subsonic to transonic attached or separated flows. This allows us to calibrate advanced fluid–structure solvers in the case of aeroelastic problems involving aerodynamics nonlinearities such as shocks and separated flows. A

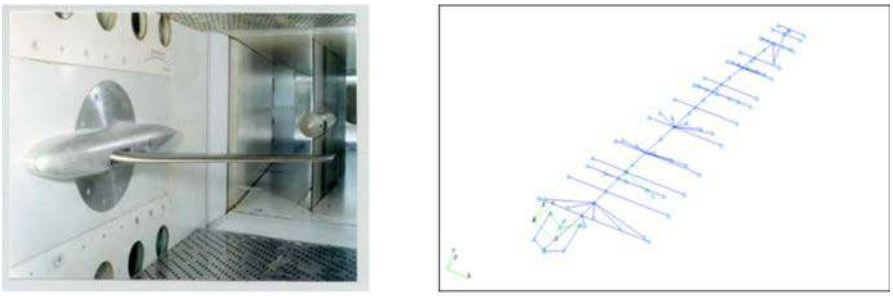

(a) (b)

Fig. 8 AMP model. **a** AMP model in the transonic ONERA wind tunnel, **b** FE structural model

structural finite element model (stick model) was developed by AIRBUS and updated with ground vibration test results (Fig. 8b).

The flutter model was designed to exhibit bending-torsion flutter in the wind tunnel behaviour, and for this reason, only the first bending mode and the first torsional mode are taken into account in the simulations. The aeroelastic full-order computational model consists of a CFD structured Euler C-mesh with 576,000 cell, which corresponds to 2,880,000 flow perturbation unknowns, and a condensed Finite Element structural model built by beam and concentrated mass. For more details, see Fig. 8b. For all simulations, the input data set, scheduled as run 208, is chosen as a reference: specifically, total pressure and total temperature are fixed, respectively, at 90,210 Pa and 298 K, the Mach number is fixed at 0.78, the angle of attack at 1.78. This data numerically give a lift coefficient equal to 0.3. The lift coefficient obtained by the wind tunnel test is 0.3. POD basis vectors are calculated using a frequency domain method of the snapshot approach. In order to compute the POD basis vectors, flow snapshots are evaluated at 13 not equally spaced reduced frequencies between 0 and 0.225 for each structural mode for a total of 52 real POD vectors (2 modes $\times$ 13 frequencies $\times$ real and imaginary part of the snapshots). A static coupling has been carried out to define the flight shape of the model.

After computation of the snapshot, the POMs vectors are calculated, and according to the energy criteria, 36 POD vectors are retained for the simulations.

The first model updating is performed using the first strategy proposed for matching of the generalized aerodynamic force obtained by POD approach and the generalized aerodynamic force obtained by the high-fidelity model. The reduced aerodynamic matrix is parameterized, as shown in Section 3, using 72 design variables r and s for each reduced frequency. The variation of the design variables is limited to 20 %, and the variation of the modified GAF is limited to 20 %. After the updating process, a check on the new unsteady pressure distribution computed is carried out to verify the correct reconstruction of the unsteady pressure field. In Fig. 6, the evaluated GAFs are compared with the reference solution: the figure shows a difference between the GAF obtained by the POD method and the GAF obtained by the high-fidelity model. After the updating process, the updated GAF is superimposed to the high-fidelity GAF. To obtain the convergence of the cost function, we need 650 iteration for a computational cost of about few seconds on a conventional desktop computer. The maximal variation of the design variable is of $+0.66$ % with respect to the original value and the minimal variation of the design variable is -0.89 % with respect to the original value (Fig. 9).

The second model updating is performed using the second strategy for all the three approaches proposed to matching the frequencies and damping of the aeroelastic system obtained by POD approach and the frequencies and damping obtained by the wind tunnel test. In particular for the experimental run 208, we have data about frequency and damping for the first structural mode for two pressure conditions and for the second structural mode for five pressure conditions, as shown in Table 2.

In order to analyse the results of the updating process more effectively, in Table 3, we propose a comparison in terms of the percentage error of the frequency and damping, after the flutter solution for six fixed pressure conditions, before the updating process and after the updating process, with respect to the experimental values.

To obtain the right convergence level ($\varepsilon <$ 1.E-04 see Fig. 3) of the objective function, we need around 2,000 iterations for a computational cost of about 13 min on a standard computer desktop. Only for the approach 1, the fixed convergence level is not reach and the updating process is stop at $\varepsilon = 0.9$. The maximal variation of the design variable found during the updating process, for the three strategies, is of $+19.25$ % with respect to the original value and the minimal variation of the design variable is -18.01 % with respect to the original value.

If we turn our attention to the frequency column, we can see that even the POD model before updating gives a very low percentage error, less than 1 %, with respect to the experimental data for the two structural modes taken into account in the simulations. Regarding the columns of the

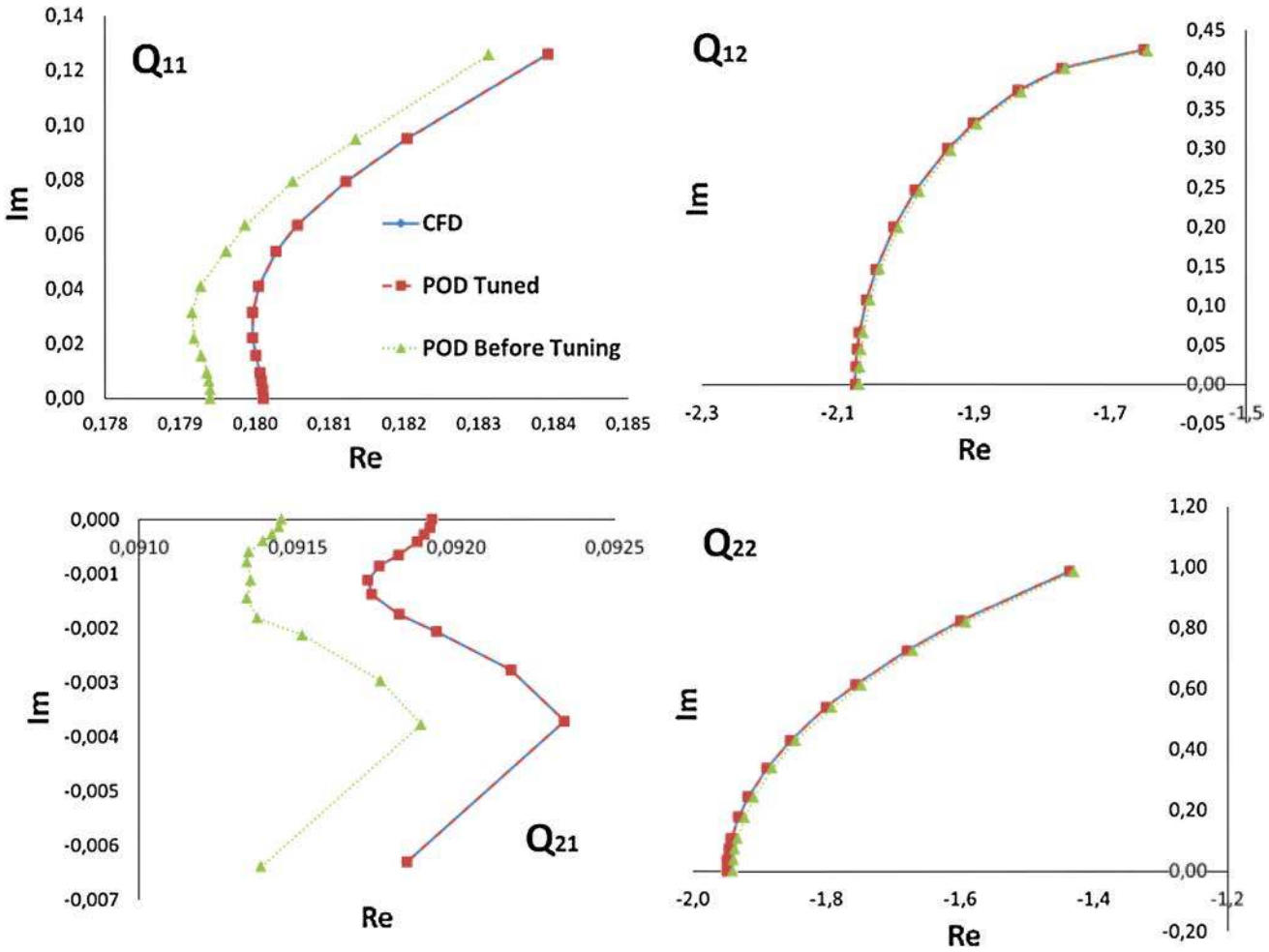

Fig. 9 GAF AMP wing comparison using Strategy 1 updating approach

Table 2 Wind tunnel experimental data (aeroelastic poles) for run 208

Pressure	Frequency exp	Damping exp
60,000	26.25	0.039
80,000	27.38	0.047
60,000	30.96	0.017
80,000	30.40	0.022
90,000	29.96	0.018
95,000	29.63	0.013
100,000	29.71	0.005

frequency after updating, we can see an improvement in terms of percentage error for the first structural mode and an augmentation of the percentage error for the second structural mode, except for the approach 3 that present a reduction of the percentage of error for the two structural modes considered. On the other hand, if we take a look at the damping column, we can see that the POD model before updating gives an important percentage error from a minimum of 10.6 % to a maximum of 79.7 % for the two structural modes. Regarding the columns of damping after updating, we can see a significant reduction of the percentage error, less than 10 % for the two structural modes (except for one pressure condition where the error is 20 %) with respect to the model before updating.

The results obtained are reported in a classical flutter plot. In Figs. 10, 11 and 12 we can see the comparison of the flutter behaviour obtained for the two structural modes taken into account in the simulations: before updating and after updating and the experimental wind tunnel test data.

For the approach 1, we can see the improvement in terms of frequency tracking for the two structural modes. Regarding the damping, as shown in Table 3, we can see the better tracking in comparison with the results obtained by the high-fidelity model before tuning.

For the approach 2, we can see the improvement in terms of frequency tracking for the first structural mode and the deterioration of the tracking for the second

Table 3 Error for poles using Strategy 2

Pressure	Error Before (%)		Error approach 1 (%)		Error approach 2 (%)		Error approach 3 (%)	
	Frequency	Damping	Frequency	Damping	Frequency	Damping	Frequency	Damping
60,000	0.42	10.60	0.18	1.19	0.19	3.78	0.30	1.59
80,000	0.75	19.99	0.07	7.69	0.39	6.43	0.36	4.54
90,000	na	na	na	na	na	na	na	na
95,000	na	na	na	na	na	na	na	na
100,000	na	na	na	na	na	na	na	na
60,000	0.59	14.84	0.68	4.12	0.56	5.55	0.06	21.01
80,000	0.95	21.98	1.09	9.34	0.94	2.31	0.01	17.18
90,000	0.92	37.29	1.62	20.30	1.16	10.16	0.03	1.97
95,000	0.27	58.64	1.44	10.06	0.98	7.45	0.24	16.37
100,000	0.83	79.74	2.05	6.50	1.69	8.53	0.70	39.54

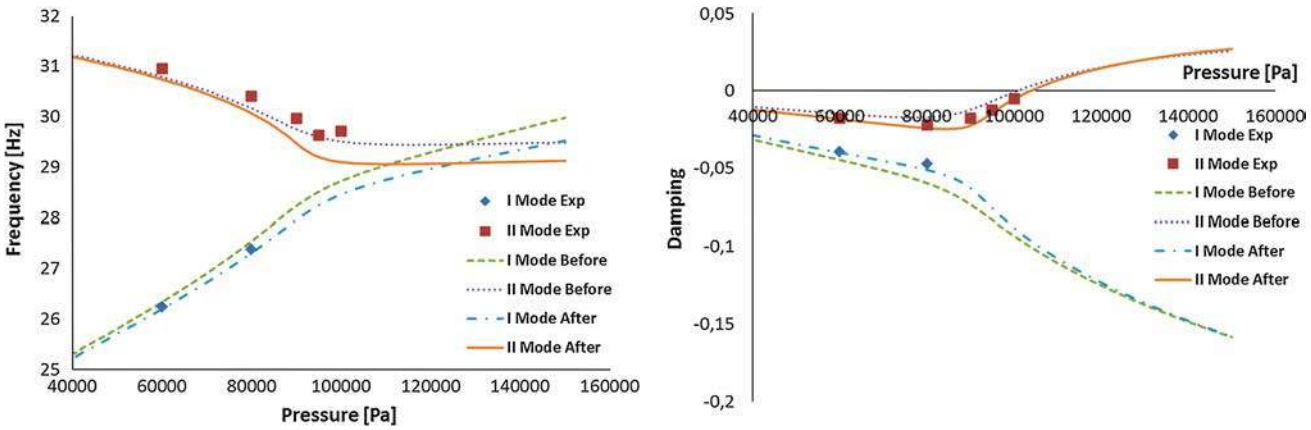

Fig. 10 GAF *flutter plot* using Strategy 2 and approach 1

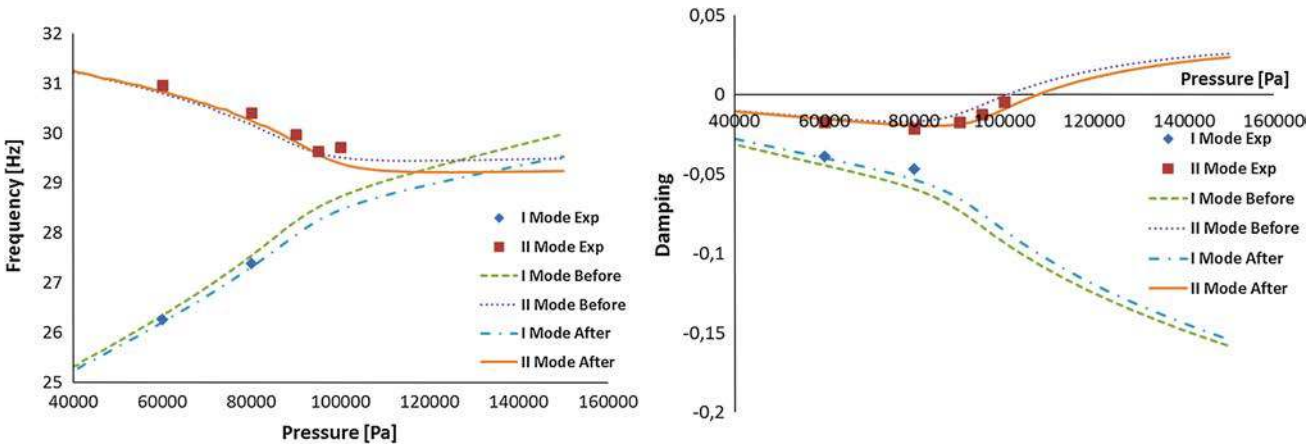

Fig. 11 GAF *flutter plot* using Strategy 2 and approach 2

structural mode. Regarding the damping, we can see the better tracking in comparison with the results obtained by the high-fidelity model.

Finally, for the approach 3, we can see the improvement in terms of frequency tracking for the first structural mode and a slight deterioration of the tracking for the second

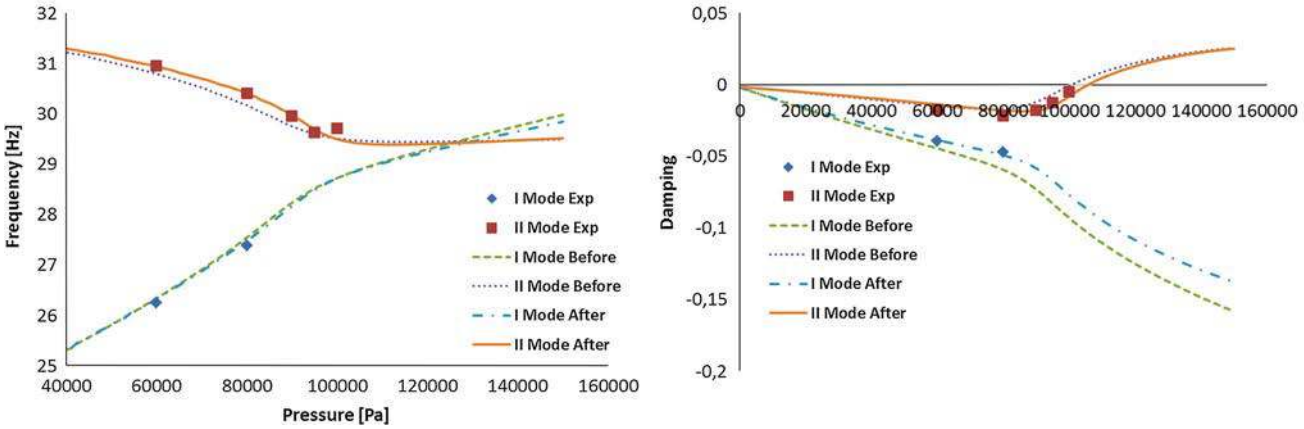

Fig. 12 GAF *flutter plot* using Strategy 2 and Approach 3

structural mode. Regarding the damping, we can see a general improvement of the results obtained by the high-fidelity model before tuning for the two structural modes.

As concluding remarks on this study, the first strategy based on the error minimization for GAF matrix gave very satisfactory updating results, but unfortunately, in the real world, experimental reference results on GAF (modal) matrix for an aircraft (or WT model) are not typically available for performing an updating process. Therefore, the second strategy directly based on a tuning minimizing the variation of the aeroelastic poles (which can be experimentally available) seems to be more effective for applications: the first approach proposed confirm a lack of accuracy due to the fact that in the objective function, only one parameter (the damping in this case) is taken into account. The approach 2 and 3 have shown a satisfactory level of accuracy with not practical differences in the resulting estimates of the aeroelastic poles in the flutter plots obtained.

5 Concluding remarks

The robustness of the accuracy of the POD approach for aeroelastic application has been demonstrated. Specifically, it is shown that the POD approach represents a very good starting point for aeroelastic application and for the updating technique for aeroelastic models. A simple method for unsteady aerodynamic model updating starting from a reduced-order model has been proposed. Two strategies on defining the model error with respect to a reference target physical behaviour and three numerical approaches have been analysed for the updating algorithm, in order to provide the highest degree of accuracy of the updated model. A critical review of the selected methods was presented, critically describing the advantages and drawbacks of the different approaches. Two aeroelastic systems were investigated: a NACA 64A010 wing section and a transonic wind tunnel model of a representative Airbus commercial aircraft. The update capabilities of the different strategies are compared in terms of GAF reconstruction in the first application and aeroelastic poles in the second example. Since the aeroelastic poles may be available by experimental wind tunnel tests (as utilized in the paper) or by flight tests, the second strategies seem to be more effective for actual application. The effectiveness of the updating strategy was validated firstly on theoretical base, with a numerical biased model, and after on application base, with wind tunnel experimental data.

Acknowledgments This paper has been supported by "Direction des Programmes Aéronautiques Civils" (DGAC/DTA/SDC).

Appendix: some details on POD basis evaluation

The starting point of the POD-based ROM procedure is calculation of the small-disturbance solution response of the fluid dynamic system at N different combinations of excitation and frequency. These solutions, also known as snapshots, are denoted by $U = \{u^n, n = 1, .., N\}$. The Euler equations, solved for the special case of an harmonic excitation of type $(M_s, t) = \underline{d}(M_s)e^{i\omega t}$, lead us to search for a solution of the form $U = \underline{U}e^{i\omega t}$, where $\underline{d}$ is a prescribed structural displacement field, ω is the frequency, and $i = \sqrt[2]{-1}$ is the imaginary number. Thus, the snapshots are the estimate of the complex unsteady field at the centre of the j th cell of the computational grid for a varying frequency ω. The POD technique is next used to find the smallest and best subspace of finite dimension $M \ll$ N which contains the dominant unsteady characteristics of the flow. The identified subspace $\{\psi^i, i = 1, .., M\}$ represent the dominate "directions" of the full original solution. Each snapshot can be approximated by a POM (proper orthogonal mode, also known as POD vectors) linear combination:

$$u^n = \bar{u} + \sum_{i=1}^{M} \eta_i \psi^i \tag{31}$$

where ψ^i are POMs and η_i are the unknown coefficients of POD expansions. The POD modes are obtained from the maximization problem:

$$\max_{\psi} \left\langle \left\| \left(u(t), \frac{\psi}{\psi} \right) \frac{\psi}{\psi} \right\|^2 \right\rangle. \tag{32}$$

We maximize the norm of the u projection on the right vectorial direction of ψ on average on T, where T is a discrete continuous set. Note that, in general, the following equivalent formulation is preferred:

$$\max_{\psi} \left\langle \frac{(u(t), \psi)^2}{(\psi, \psi)} \right\rangle. \tag{33}$$

The previous maximum problem for a definite-positive function is equivalent to the resolution of the following eigenvalues problem

$$\mathrm{SV} = V\sigma^2 \tag{34}$$

where S is the real snapshot correlation matrix

$$S = \mathrm{RR}^T \tag{35}$$

with,

$$R = (Re(U) Im(U)) \tag{36}$$

and each column of U contains a complex valued snapshot. V is an eigenvector. Note that the corresponding eigenvalues are expected to be positive because of the positiveness of the matrix S, and therefore, the positive quantity σ^2 is directly introduced in Eq. 34.

The choice of the eigenvector to build the POD basis is made according to the following criteria:

1. Snapshots that are not decorrelated: the modes obtained from decorrelated snapshots are the snapshots themselves and they all have the same eigenvalues.
2. Elimination of the eigenvectors associated with eigenvalues that are zero or too small.
3. There is a little difference between the partial and total energy.

As shown in Ref. [15], the POMs are simply a linear rearrangement of the original snapshot:

$$\psi^i = \sum_{n=1}^{n} a_m^i u^n \tag{37}$$

After the eigenvalues problem (Eq. 34) has been solved, the POMs are computed by the Eq. (37) where

$$a_m^i = V_M \sigma_M^{-1}. \tag{38}$$

References

1. Mortchelewicz, G.D.: Application of proper orthogonal decomposition to linearized Euler or Reynolds-Averaged Navier-Stokes equation. In: 47th Israel Annual Conference on Aerospace Sciences, Tel Aviv, February 2007. http://publications.onera.fr/
2. Palacios, R., Climent, H., Karlsson, A., Winzell, B.: Assessment of strategies for correcting linear unsteady aerodynamics using CFD or test results. In: International Forum of Aeroelasticity and Structural Dynamics, Madrid, June 2001
3. Giesing, J.P., Kalman, T.P., Rodden, W.P.: Correction factor techniques for improving aerodynamic prediction method. Technical report NASA CR-144967 (1976)
4. Yates, E.C.: Modified-strip-analysis method for predicting wing flutter at subsonic or hypersonic speeds. J. Aircr. **3**(1), 25–29 (1966)
5. Pitt, D.M., Goodman, C.E.: Flutter calculations using Doublet Lattice Aerodynamics modified by the full potential equations. In: 28th AIAA/ASME/ASCE/AHS Structures, Structural Dynamics and Materials Conference, Monterrey, 1987 (Paper AIAA-87-0882-CP)
6. Baker, M.L.: CFD based corrections for linear aerodynamic methods, AGARD R822, October 1997
7. Schulze, S., Tichy, L.: An efficient aero-correction method for transonic flutter calculations, DASA B08/98
8. Pak, C.: Unsteady aerodynamic model tuning for precise flutter prediction. J. Aircr. **48**(6), 2178–2184 (2011)
9. Hu, P., Qu, K., Xue, L., Ni, K., Dowell, E.: Efficient aeroelastic model updating in support of flight testing. In: AIAA Atmospheric Flight Mechanics Conference, Chicago, August 2009 (AIAA-2009-5713)
10. Thomas, J.P., Dowell, E.H., Hall, K.C.: Three-dimensional transonic aeroelasticity using proper-orthogonal decomposition-based reduced-order models. J. Aircr. **40**(3), 544–551 (2003)
11. Bui-Thanh, T., Damodaran, M., Willcox, K.: Proper orthogonal decomposition extensions for parametric applications in transonic aerodynamics. In: 21st AIAA Applied Aerodynamics conference, Orlando, June 2003 (AIAA Paper 2003-4213)
12. Lind, R., Brenner, M.: Incorporating flight data into a robust aeroelastic model. J. Aircr. **35**(3), 470–477 (1998)
13. Maute, K., Nikbay, M., Farhat, C.: Coupled analytical sensitivity analysis and optimization of three-dimensional nonlinear aeroelastic systems. AIAA J. **39**(11), 2051–2061 (2011)
14. Giunta, A.A.: Sensitivity analysis for coupled aero-structural systems. In: NASA Technical memorandum, Hampton, August 1999 (NASA/TM-1999-209367)
15. Thomas, J.P., Hall, K.C., Dowell, E.H.: Reduced-order modelling of unsteady small-disturbance flows using a frequency-domain proper orthogonal decomposition technique. In: 37th AIAA Aerospace Sciences Meeting and Exhibit, Reno, January 1999 (AIAA 99-655)
16. Xiao, M., Breitkopf, P., Filomeno Coelho, R., Knopf-Lenoir, C., Villon, P.: Constrained proper orthogonal decomposition based on QR-factorization for aerodynamical shape optimization. Appl. Math. Comput. (2013). doi:10.1016/j.amc.2013.07.086
17. Fang, F., Pain, C.C., Navon, I.M., Gorman, G.J., Piggott, M.D., Allison, P.A., Goddard, A.J.H: A POD goal-oriented error measure for mesh optimisation. Int. J. Numer. Methods Fluids **63**, 185–206 (2010)
18. Mortchelewicz, G.D.: Flutter simulations. Aerospace Sci Technol **4**(1), 33–40 (2000). ISSN 1270-9638. http://dx.doi.org/10.1016/S1270-9638(00)00116-4
19. Zona Technology Inc.: ZAERO Theoretical Manual, June 2011

20. Mortchelewicz, G.D.: Aircraft aeroelasticity computed with linearized RANS equations. In: 43rd Israel Annual Conference on Aerospace Sciences, Tel Aviv, February 2003. http://publications.onera.fr/
21. Carlberg, K., Farhat, C.: A low-cost, goal-oriented 'compact proper orthogonal decomposition' basis for model reduction of static system. Int. J. Numer. Meth. Eng. **86**, 381–402 (2011). doi:10.1002/nme.3074
22. Filomeno Coelho, R., Breitkopf, P., Knopf-Lenoir, C.: Bi-level model reduction for coupled problems. Application to a 3D wing. Struct. Multidiscipl. Optim. **39**(4), 401–418 (2009). doi:10.1007/s00158-008-0335-3
23. Lucia, D.J., Beran, P.S., Silva, W.A.: Reduced-order modelling: new approaches for computational physics. Progr. Aerospace Sci. **40**(1–2), 51–117 (2004). doi:10.1016/j.paerosci.2003.12.001
24. Vetrano, F., le Garrec, C., Mortchelewicz, G.D., Ohayon, R.: Assessment of strategies for interpolating POD based reduced order model and application to aeroelasticity. J. Aeroelast. Struct. Dyn. **2**(2), 85–104 (2011)
25. Gill, P.E., Murray, W., Saunders, M.A.: User's Guide for SNOPT Version 7: Software for Large-Scale Nonlinear Programming, February 2006
26. Zingel, H. et al.: Measurement of steady and unsteady air loads on a stiffness scaled model of a modern transport aircraft wing. In: International Forum on Aeroelasticity and Structural dynamics, Aachen, June 1991. DGLR 91-06, pp. 120–131 (1991)